arXiv:hep-ex/0206007 v1   3 Jun 2002

Optimizing the Linear Collider Detector for the Measurement of the Higgs to Charm Branching Ratio*

TOSHINORI ABE and AARON S. CHOU
Stanford Linear Accelerator Center, 2575 Sand Hill Road,
Menlo Park, CA, USA†

Abstract

Several different vertex detector designs for the Linear Collider Detector (LCD) are evaluated in the context of measurements of the branching ratio of the standard model Higgs particle decaying into charm/anti-charm final states. Fast Monte Carlo simulations are used to model the detector and neural network-optimized flavor tagging is used to perform the measurements. These tools are used to study the effects of pixel resolution, material thickness, and inner layer radius on the flavor tagging efficiency-purity curve and ultimately on the branching ratio measurement error.

1 Introduction

A worldwide effort is now underway to develop a future Linear Collider and a corresponding Linear Collider Detector (LCD). Compromises may have to be made in the design of such a detector between its desired performance and other considerations such as the restrictions imposed by beam-related backgrounds in the interaction region as well as the total cost of the detector. In this paper, we use Monte Carlo simulations to model the performance of various detector configurations in the contexts of flavor tagging and sensitivity in the measurement of the branching ratio of a 120 GeV Higgs boson to charm/anti-charm final states. Such a measurement would help determine whether the condensation of a single Higgs boson is sufficient to generate the masses of particles. The dependence of the measurement precision on the various detector parameters used provides useful data for optimizing the final design of the detector.

The branching ratios $BR(H^0 \to c\bar{c})$ and $BR(H^0 \to b\bar{b})$ may be simultaneously measured using the SLD technique [1] for measuring the the analogous quantities R_b and R_c in Z^0 decays. The branching ratios may be measured by performing flavor tagging and then counting the number of

---

*Talk presented by A.C. at the Linear Collider Workshop at the University of Chicago, January 7-9, 2002.

†Work supported in part by Department of Energy contract DE-AC03-76SF00515.

b-tagged, c-tagged, and untagged decays. These data can then be unfolded using the flavor tagging efficiency matrix.

Efficient and pure flavor tagging requires precise impact parameter resolution in order to distinguish heavy flavor decay tracks from fragmentation tracks from the primary interaction point (IP). This tracking resolution may be written as $\sigma_0 \oplus \sigma_{MS}/(p \cdot \sin^{3/2} \theta)$ for a cylindrically symmetric detector where θ is measured from the z axis and p is the particle's momentum. σ_0 is the asymptotic resolution at infinite momentum and it scales linearly with the detector's single hit resolution. For finite momentum, the total resolution is usually dominated by the second term where σ_{MS} includes the effects of multiple Coulomb scattering and thus scales as the square root of the detector layer thickness. Both errors scale roughly linearly with the inner radius of the detector which is effectively the extrapolation distance from the innermost hit inward to the IP. The effects of variations of these three detector parameters on flavor tagging are described below. Most of the same assumptions are made as in a previous study of the same topic by the University of Oregon group[2], and our results are very consistent with theirs. However, the current study explores several additional detector configurations.

2 The Analysis Tools

The various vertex detector configurations are simulated using the LCDTRK program[3] which, given an input detector geometry, generates smearing tables for the track parameter error matrices. Non-Gaussian measurement errors are not modelled. These smearing tables are input into the LCDROOT[4] package for the event generation and fast MC detector simulation.

To calibrate the fast MC, the SLD tracking resolution is simulated by replacing the tracking chambers of the small detector (SDMAR01)[5] with a model of the SLD tracking chambers [6] [7] [8] . This model is tuned to reproduce the measured SLD track position resolution of $\sim (9 \oplus 33/((p/\text{GeV}) \cdot \sin \theta^{3/2})$ μm. For this tuning, the beampipe thickness is increased from $0.52\% \, X^0$ to $0.65\% \, X^0$ in order to accomodate the increased measurement error from Rutherford scattering tails. The magnetic field for the drift chamber is set to 0.6 T and interaction point (IP) measurement errors $(4 \cdot 4 \cdot 20)\mu$m are modelled by smearing the MC IP position. 20K Z^0 pole hadronic decay events are generated and the LCDJetFinder and LCDVToplGhost packages in LCDROOT are used to find jets using the Durham algorithm, and to perform topological vertexing [9] [10] within the jets.

A jet flavor tag analogous to the SLD method[11] is then developed. The tag proceeds in three stages, each of which is optimized with the Stuttgart neural network trainer. First, the best candidate b vertex is selected from the vertices found in the jet. This selection is based on the vertex flight distance, the flight distance normalized by the vertex measurement error, the angle of the vertex flight direction with respect to the jet axis, the number of tracks in the vertex, and the raw vertex mass computed from the track momenta.

Next, tracks are attached to the b vertex using the following criteria: the transverse distance

of the track to the vertex flight axis at the point of closest approach ($POCA$), the longitudinal distance of the $POCA$ on the vertex flight axis to the IP, this longitudinal distance divided by the vertex flight distance, the angle of the track momentum with respect to the vertex flight direction, and the track impact parameter normalized by its measurement error. The vertex kinematics are then recalculated using all of the attached tracks.

Finally, the jet flavor is identified using the P_T-corrected vertex mass, the vertex momentum, the vertex flight distance, the flight distance normalized by the vertex measurement error, the number of vertices found, and the number of 1-prong vertices found. The results of the jet flavor tag are shown in figure 1. These efficiency-purity curves are very similar to the the flavor tag results of the full SLD MC shown in figure 2. The fast MC b tag has slightly lower purity perhaps because the 'ghost track' vertexing algorithm used in the fast MC tag instead of the 'resolubility' vertexing algorithm used in the SLD tag. The 'ghost' algorithm is more susceptible to creating vertices from poorly measured fragmentation tracks, thus incorrectly increasing the vertex mass. The discrepancy is very small however, and we conclude that the fast MC using LCDTRK and LCDROOT is sufficiently good for our purposes.

3 Flavor Tagging in Higgstrahlung Events

To measure the various Higgs branching fractions, we look at Higgstrahlung events in which the final state Z^0 is identified by reconstructing its decay into e^+e^- or $\mu^+\mu^-$ and a 120 GeV Higgs is identified through its recoil mass. The efficiency of the recoil mass technique to tag a 120 GeV Higgs is estimated to be $\sim 31\%$ with $\sim 44\%$ impurity from Z^0Z^0 events due to degradation of the beam energy constraint from beamstrahlung and initial state radiation. To reduce the $Z^0 \rightarrow c\bar{c}$ background, a cut of $|\cos\theta| < 0.6$ is imposed on the jet axes to remove a large fraction of the polarized Z^0's produced by the 80% polarized electron beam. The resulting Higgs efficiency is $\sim 19\%$ with 75% purity. Since only leptonic decays of the Z^0 are used, the Higgs decay jets can be selected unambiguously in this study, but only $\sim 6\%$ of the Higgstrahlung events can then be used. However, jets from Higgs and hadronic Z^0 decays can be separated some fraction of the time, and so the fraction of usable events in a full analysis can very likely be increased by a factor of 4. Assuming a 60 fb Higgstrahlung cross-section, the total number of usable tagged Higgs decays in a 500 fb^{-1} sample is then estimated to be:

$$N_H \approx 500 \text{ fb}^{-1} \cdot 60 \text{ fb} \cdot 0.19 \cdot 0.06 \cdot 4 \approx 1370. \tag{1}$$

For each detector configuration, 20K Higgstrahlung events are generated in which the Z is forced to decay into e^+e^- or $\mu^+\mu^-$ and the 120 GeV Higgs decays hadronically. Since the branching ratio $BR(H \rightarrow c\bar{c})$ is expected to be low, to get a good statistical sample of charm jets, an additional 20K Higgstrahlung events are generated in which the Higgs are now forced to decay to $c\bar{c}$. The magnetic field is set to 5 Tesla.

3

The IP position measurement is modelled to have $(4 \times 4 \times 6)\mu$m resolution. These numbers are motived by the SLC IP position measurement[12] which is composed of measurements of the beam position averaged over many events, and an event-by-event measurement of the longitudinal position along the beam of the primary vertex. The SLC beam position is measured by putting fragmentation tracks from 30 consecutive hadronic events into a common 2D vertex in order to average over the jet axis distribution in ϕ. At luminosities of 10^{34} cm^{-2} sec^{-1} the event rate for $W^{+}W^{-}$ and $Z^{0}\gamma$ events at the Linear Collider should be comparable to the Z^{0} event rate (~ 200/hour) at the SLC, and this technique should still work provided that the beam does not move by more than a few microns per hour. The SLC longitudinal IP position is measured event-by-event using the point of closest approach to the beam of the median track in the track-to-beam impact parameter distribution of tracks in the event. The resolution of this technique is expected to be of the same order as the average track position resolution. The changes in the longitudinal IP resolution when using different detector configurations have been neglected and so the changes in the branching ratio measurement precision for the most extreme detector configurations in table 1 may be slightly underestimated.

The vertex selection and track attachment neural networks are trained only once for the standard SDMAR01 configuration[5], but the jet flavor tagging neural net is retrained using these 40K events for each new detector configuration. 20K of the events are used for training and 20K for validation to avoid overtraining. The same training regimen is used for each configuration: 1000 cycles of standard backpropagation with the learning rate set to 0.2 and then 1000 cycles each of backpropagation with momentum 0.5 and the learning rate set to 0.1, 0.05, and 0.01. Studies showed that additional training beyond this basic regimen yield only marginal improvements in the flavor tagging. Small improvements could also be made using a 300K event sample for the training, but working with such large sample sizes was not feasible for this quick study.

Since each hadronic Higgs decay produces both a quark jet and an anti-quark jet, there are two chances to tag the decay type. The event level flavor tag may be defined as follows. If either or both jets are b-tagged, then the event is b-tagged. If either or both jets are c-tagged and neither is b-tagged, then the event is c-tagged. Otherwise, the event is untagged and considered to be a decay into light quarks. For example, the event flavor tagging efficiencies $\mathbf{E} \equiv E_{ij}$ for identifying flavor i as flavor j may be expressed in terms of the jet flavor tagging efficiencies ϵ_{ij} as:

$$
\begin{aligned}
E_{cc} &= \epsilon_{cc}^2 + 2\epsilon_{cc} \cdot \epsilon_{cu} \\
&= 2 \cdot \epsilon_{cc} \cdot (1 - \epsilon_{cb}) - \epsilon_{cc}^2 \qquad (2) \\
E_{bc} &= \epsilon_{bc}^2 + 2\epsilon_{bc} \cdot \epsilon_{bu} \\
&= 2 \cdot \epsilon_{bb} \cdot (1 - \epsilon_{bb}) - \epsilon_{bc}^2 \qquad (3)
\end{aligned}
$$

Here, the unitarity of the jet flavor tagging efficiency matrix is used for the second equality and i and j take on values of b, c and u for untagged. Values of $\epsilon_{bb} \approx 0.6$ and $\epsilon_{cb} \approx 0.02$ are typical. In these formulae, the effects on flavor tagging due to energy correlations between the two jets in a decay are neglected. However, since the $BR(H \to c\bar{c})$ measurement is dominated by the $H \to b\bar{b}$

background, these correlations can only improve the measurement by reducing E_{bc} by making it less likely that the two b jets are both tagged as c.

4   Measuring the Branching Fractions

The branching ratios $\mathbf{BR_H} \equiv (BR_{H \to b\bar{b}}, BR_{H \to c\bar{c}}, BR_{H \to u\bar{u}})$ may be extracted by counting the number of event level flavor tags of each flavor $\mathbf{T} \equiv (T_b, T_c, T_u)$ by solving the matrix equation:

$$\mathbf{T} = \mathbf{E} \cdot (\mathbf{BR_H} \cdot N_H + \mathbf{BR_Z} \cdot N_Z) \tag{4}$$

to get:

$$\Delta \mathbf{BR_H} = \mathbf{E}^{-1} \cdot (\mathbf{T} - \mathbf{E} \cdot \mathbf{BR_Z} \cdot N_Z)/N_H \tag{5}$$

Here, N_H and N_Z are the numbers of Higgs and Z^0's in the Higgs-tagged sample, and the Z^0 decay branching ratios $\mathbf{BR_Z}$ are defined in the same manner as $\mathbf{BR_H}$. The flavor tagging efficiency is assumed to be largely independent of whether a jet originated from a Higgs decay or from a Z^0 decay. This assumption may need to be revised when considering Higgs masses much larger than the Z^0 mass.

Neglecting the error in the efficiency matrix (measured by counting the mixed tag rates where one jet is tagged as flavor i and the other as flavor j) and the error from subtracting the Z^0 background (presumably measured from the shape of the recoil mass distribution), the branching ratio error may be estimated as:

$$\Delta \mathbf{BR_H} \approx \mathbf{E}^{-1} \cdot \sqrt{\mathbf{T}}/N_H \tag{6}$$

In particular, if the Poisson fluctuations ΔT_b and ΔT_u are ignored then for Higgs to $c\bar{c}$ decays:

$$\Delta BR_{H \to c\bar{c}} \approx E_{cc}^{-1} \cdot \sqrt{T_c}/N_H \tag{7}$$

The number of c-tagged events is estimated as

$$T_c \approx (E_{cc} \cdot BR_{H \to c\bar{c}} + E_{bc} \cdot BR_{H \to b\bar{b}}) \cdot N_H + E_{cc} \cdot BR_{Z \to c\bar{c}} \cdot N_Z \tag{8}$$

where the small contamination from $BR_{Z \to b\bar{b}}$ is ignored. The fractional measurement error is then:

$$\frac{\Delta BR_{H \to c\bar{c}}}{BR_{H \to c\bar{c}}} \approx \frac{\sqrt{E_{cc} \cdot BR_{H \to c\bar{c}} + E_{bc} \cdot BR_{H \to b\bar{b}} + E_{cc} \cdot BR_{Z \to c\bar{c}} \cdot N_Z/N_H}}{E_{cc} \cdot BR_{H \to c\bar{c}} \cdot \sqrt{N_H}} \tag{9}$$

It is estimated that the Higgs tag has 75% purity and so $N_Z/N_H \approx 0.33\%$. It is also assumed that the true values of the branching ratios are: $BR_{H \to c\bar{c}} = 3\%$, $BR_{H \to b\bar{b}} = 72\%$, and $BR_{Z \to c\bar{c}} = 12.4\%$.

In figures 5- 9 below, for various vertex detector configurations listed in table 1, the efficiency-purity curve of the event flavor tag is plotted. These curves are generated by varying the value of the cut on the neural network output. The scaled precision P, defined as:

$$P = \sqrt{N_H} \cdot \Delta BR_{H \to c\bar{c}} / BR_{H \to c\bar{c}} \tag{10}$$

is also plotted as a function of the event flavor tagging point chosen on the efficiency-purity curve. This quantity is a measure of the analyzing power and can be divided by $\sqrt{N_H} \approx \sqrt{1370} \approx 37$ for a 500 fb^{-1} data set to get the fractional branching ratio error.

For example, for the standard SDMAR01 configuration with 5 μm hit resolution and 0.12% X^0 thickness and inner radius 1.2 cm, figure 5 indicates that the best precision occurs at $E_{cc} \approx 0.66$ and $E_{bc} \approx 0.06$ and the relative branching fraction error can be calculated to be $\Delta BR_{H \to c\bar{c}} / BR_{H \to c\bar{c}} \approx 13.8/37 \approx 0.37$. For $N_H \approx 1370$ and $N_Z \approx 452$, the breakdown of the tagged charm events is ~ 27 correct tags from $H^0 \to c\bar{c}$, ~ 59 mistags from $H^0 \to b\bar{b}$, and ~ 36 correct background tags from $Z^0 \to c\bar{c}$. The mistags from $Z^0 \to b\bar{b}$ are neglected. Our result is very consistent with that of the Oregon result[2] of $\Delta BR_{H \to c\bar{c}} / BR_{H \to c\bar{c}} \approx 0.39$ for the same model.

5   The Results

The single hit resolution σ_{res} is varied (figure 5) between 1μm and 10μm to cover resolutions ranging from CCD pixel detectors and of silicon strip detectors. For example, changing from the 5μm resolution SDMAR01 detector to a 1μm detector only decreases the error by a factor of $13.3/13.8 = 0.964$. The changes in precision may be estimated as $\Delta P/\Delta\sigma_{res} \approx 0.12 \ \mu$m^{-1}.

A large range of variations is chosen for the detector layer thickness t, from $0.03\% X^0$ to $1.00\% X^0$ again to model anything from the thinnest CCD structures to silicon strips (with readout electronics electronics on the ends). These variations, shown in figure 6 resulted again in changes of precision of magnitude similar to those of the single hit resolution variations. These changes may be roughly parameterized as $\Delta P/\Delta\sqrt{t} \approx 1.38$ where t is measured in $\% X^0$. The larger effects of simultaneous variations in both single hit resolution and layer thickness are shown in figure 7.

The dependence on the vertex detector inner radius R_0 is shown in figure 8. Not much difference can be seen, and the dependence is approximately $\Delta P/\Delta R_0 \approx 0.17/$cm. This result indicates that it may be possible to increase the detector inner radius to better avoid the e^+e^- pair backgrounds without sacrificing much precision in the branching ratio measurement.

Finally, the dependence of the measurement on the center-of-mass energy is shown in figure 9 for $\sqrt{s} = 250, 500$ GeV for two different detector configurations. Changing the energy appears to have only small effects on the flavor tagging contribution to the measurement precision. Perhaps more important are the effects of different Standard Model backgrounds to the Higgs tag at the two different energies which have not been modelled in this study.

hit res. [μm]	thickness [% X_0]	inner radius [cm]	σ_0 [μm]	σ_{MS} [μm·GeV/c]
10.0	0.12	1.2	4.7	11.7
5.0	0.12	1.2	2.5	8.0
1.0	0.12	1.2	0.7	4.8
5.0	1.00	1.2	2.5	16.0
5.0	0.03	1.2	2.5	6.0
10.0	1.00	1.2	4.7	20.4
1.0	0.03	1.2	0.7	3.1
5.0	0.12	2.4	2.6	12.7
(SLD) 4.0	0.40	2.8	9.0	33.0

Table 1: The different detector configurations based on variations of SDMAR01 and the corresponding track position resolution, $\sigma_0 \oplus \sigma_{MS}/(P \cdot \sin^{3/2}\theta)$. The last entry represents the SLD model which has an enhanced 0.65% X^0 beampipe at 2.5 cm radius and has the SDMAR01 tracking chambers replaced with a model of the SLD vertex detector and central drift chamber. All other models have a 0.04% X^0 beampipe at 1.0 cm radius.

6   Conclusion

In this study, we have found that the precision of a $BR(H^0 \to c\bar{c})$ measurement is only modestly dependent on the variations of several detector parameters. This small dependence can be explained by the fact that the base configuration (SDMAR01) already provides exceedingly good tracking resolution. Even the worst detector configuration modelled offers resolution much better than that of any existing vertex detector. The modelled tracking resolutions (shown in table 1) are much smaller than the distance scales given by the lifetimes of weakly decaying heavy hadrons, for example $c\tau_D \approx 140\mu$m. Flavor tagging analyses are therefore able to cut deeply into the exponential impact parameter distribution to achieve a high efficiency for separating heavy flavor decay tracks from fragmentation tracks. Further improvements in detector precision can only hope to recover the small remaining fraction of the exponential distribution at low proper time.

It therefore does not seem necessary from the standpoint of flavor tagging to attempt to go to extraordinary lengths to achieve further improvements in resolution. However, other applications of precision tracking still need to be studied. For example, in measurements of parity violation or CP violation in new physics sectors or even at the Z^0 pole in a giga-Z^0 run, it is necessary to determine not just the particle species, but also its charge. Even if a newly discovered particle does not have a weak decay scale lifetime, its charge may be measured if it decays to a b or c hadron. In either case, the loss of even a single secondary decay track creates an impurity in the charge measurement. It is therefore expected that these types of measurements may be more sensitive to changes in the tracking resolution.

References

[1] **SLD** Collaboration, K. Abe *et al.*, "A measurement of R(c) using the SLD detector," `SLAC-PUB-7880`. Talk given at 29th International Conference on High-Energy Physics (ICHEP 98), Vancouver, Canada, 23-29 Jul 1998.

[2] J. E. Brau, C. Potter, and M. Iwasaki, "Linear collider vertex detector optimization for Higgs branching ratio measurements,".

[3] B. A. Schumm, "Tracking and vertexing at a high energy linear collider," `hep-ex/9909054`.

[4] T. Abe and M. Iwasaki, "The LCDROOT analysis package," `hep-ex/0110068`.

[5] **American Linear Collider Working Group** Collaboration, T. Abe *et al.*, "Linear collider physics resource book for Snowmass 2001. 4: Theoretical, accelerator, and experimental options," `hep-ex/0106058`.

[6] K. Abe *et al.*, "Design and performance of the SLD vertex detector, a 307 Mpixel tracking system," *Nucl. Instrum. Meth.* **A400** (1997) 287–343.

[7] M. D. Hildreth *et al.*, "Performance of the SLD central drift chamber," *IEEE Trans. Nucl. Sci.* **42** (1995) 451.

[8] M. J. Fero *et al.*, "Performance of the SLD central drift chamber," *Nucl. Instrum. Meth.* **A367** (1995) 111–114.

[9] D. J. Jackson, "A topological vertex reconstruction algorithm for hadronic jets," *Nucl. Instrum. Meth.* **A388** (1997) 247–253.

[10] **SLD** Collaboration, K. Abe *et al.*, "Time dependent B/s0 - anti-B/s0 mixing using inclusive and semileptonic B decays at SLD," `hep-ex/0012043`.

[11] P. C. Rowson, D. Su, and S. Willocq, "Highlights of the SLD physics program at the SLAC Linear Collider," *Ann. Rev. Nucl. Part. Sci.* **51** (2001) 345–412, `hep-ph/0110168`.

[12] A. S. Chou, "B decay charm counting via topological vertexing," tech. rep., SLAC, 2001. SLAC-R-578.
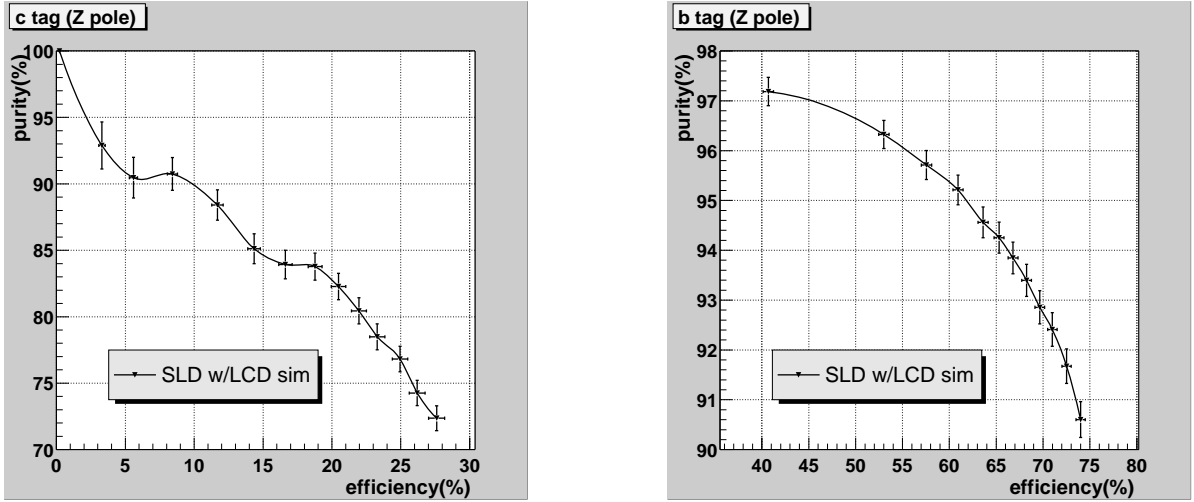
Figure 1: The efficiency-purity curves of the LCDROOT fast MC jet b-tag (left) and c-tag (right) for the SLD detector. The 'ghost track' algorithm is used for vertexing.
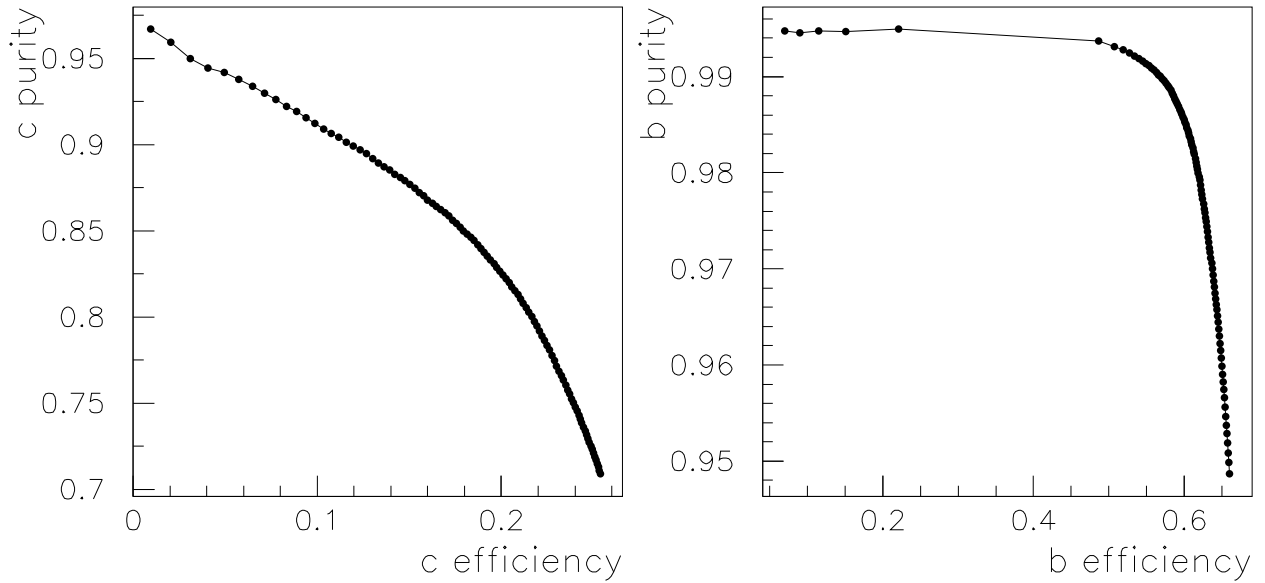

Figure 2: The efficiency-purity curves for the full MC jet c-tag (left) and b-tag (right) for the SLD detector. The 'resolubility' algorithm is used for vertexing.
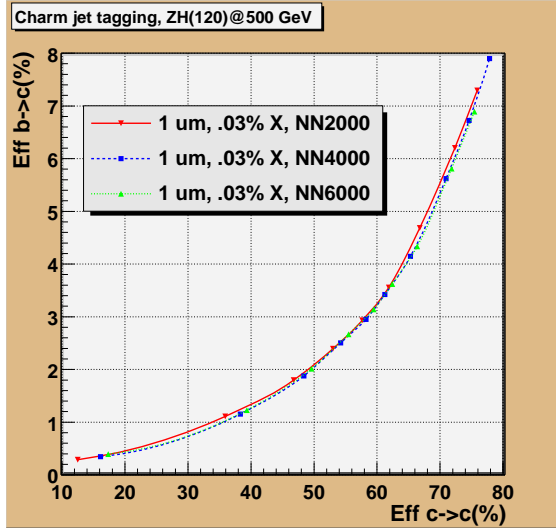
9

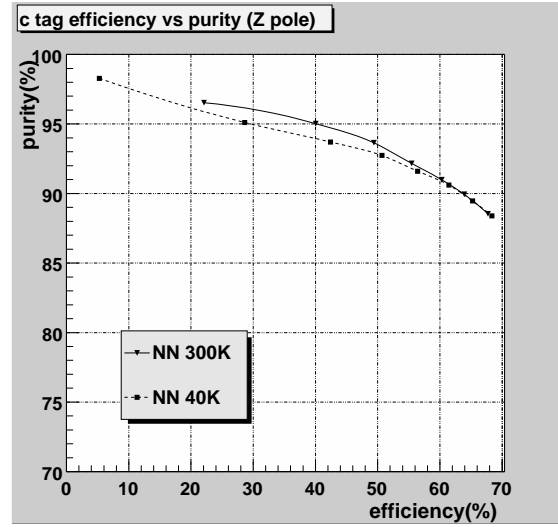Figure 3: The $b \to c$ mistag rate versus the $c \to c$ correct tag rate of the jet flavor tag for different numbers of neural network training cycles.

Figure 4: The efficiency-purity curve of the jet flavor tag for neural networks trained with 300K Z^0 events and with 40K Z^0 pole events.
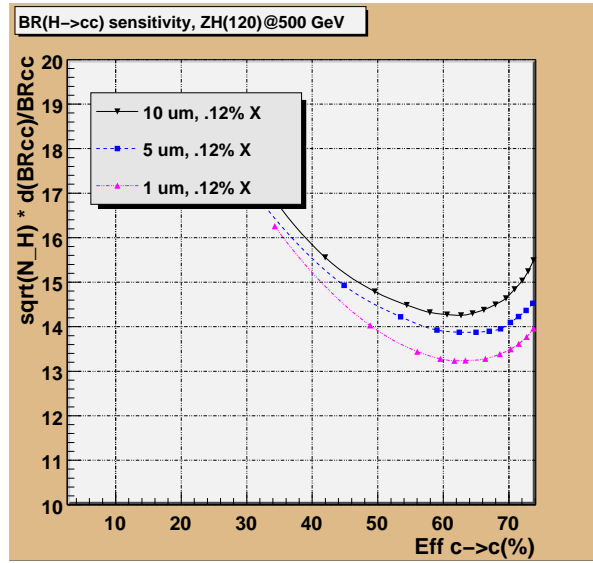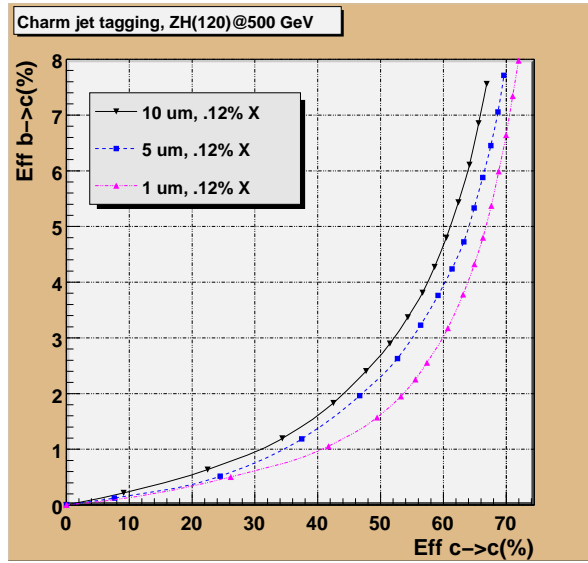

Figure 5: (Left) The event mistag rate E_{bc} versus the event correct tag rate E_{cc} for vertex detectors of different hit resolution but the same layer thickness of 0.12% X^0 and the same inner radius of 1.2 cm. (Right) The corresponding fractional $BR(H \to c\bar{c})$ precision.
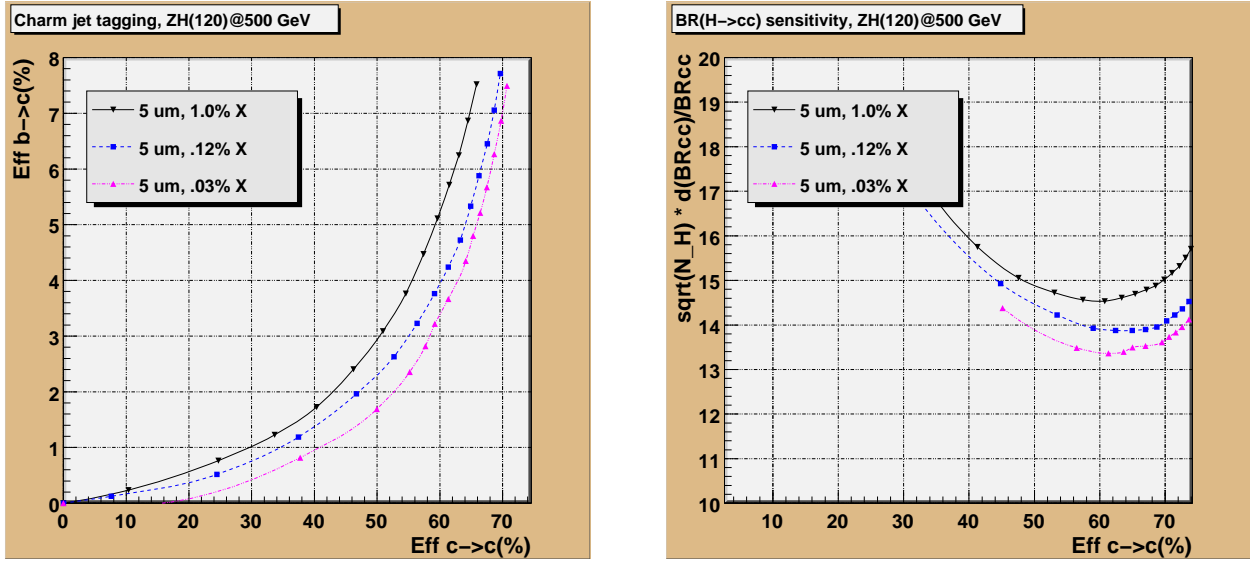
10

Figure 6: (Left) The event mistag rate E_{bc} versus the event correct tag rate E_{cc} for vertex detectors of different layer thickness but the same hit resolution of 5 μm and the same inner radius of 1.2 cm. (Right) The corresponding fractional $BR(H \to c\bar{c})$ precision.
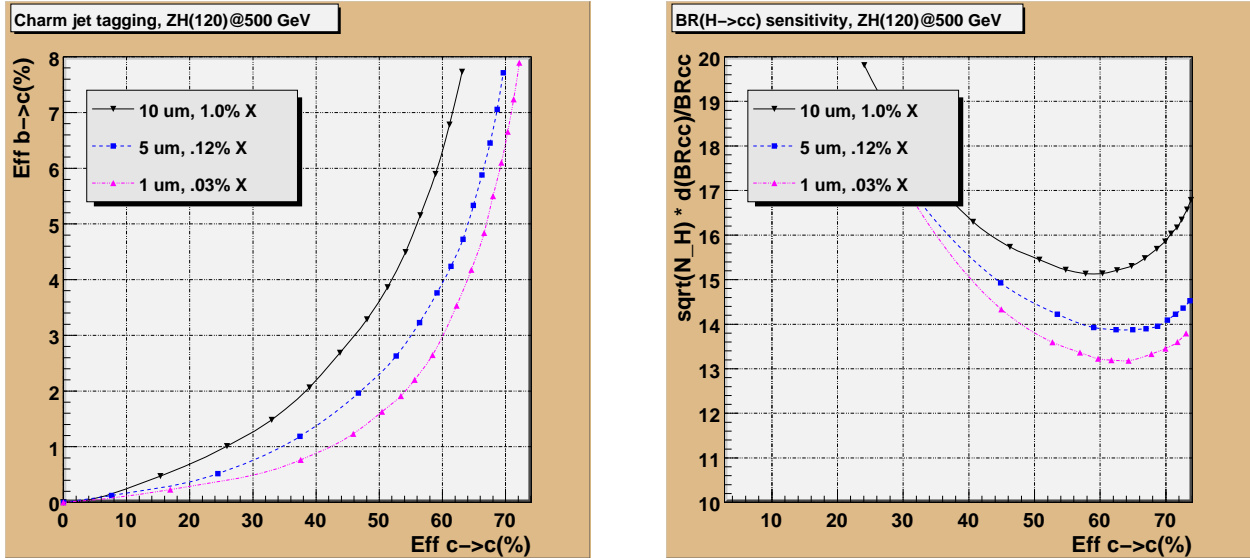

Figure 7: (Left) The event mistag rate E_{bc} versus the event correct tag rate E_{cc} for vertex detectors of different layer thickness and different hit resolution but the same inner radius of 1.2 cm. (Right) The corresponding fractional $BR(H \to c\bar{c})$ precision.
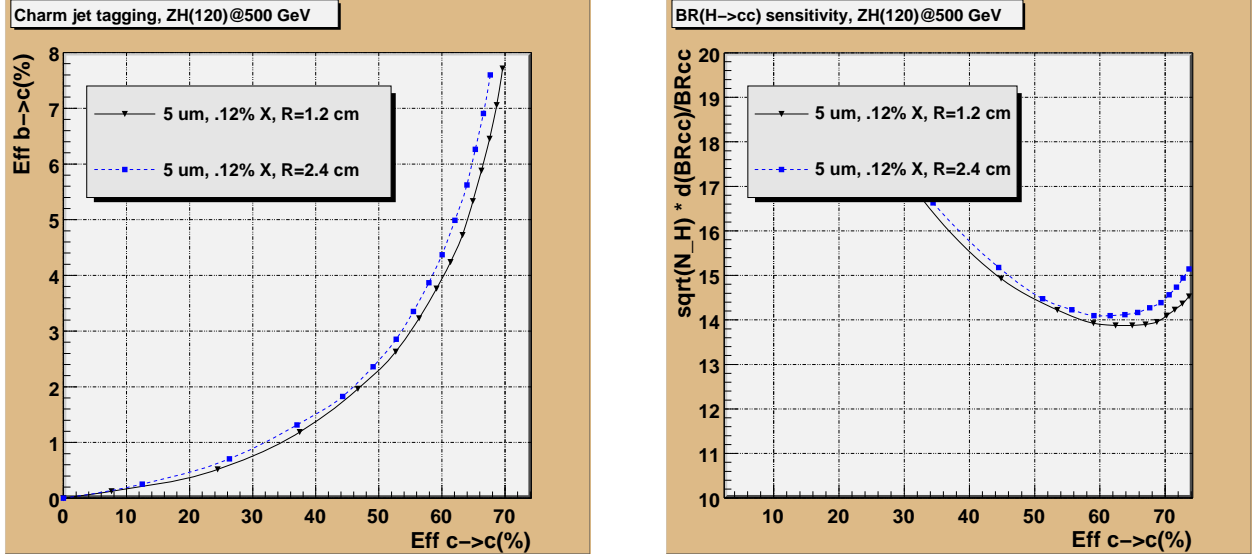
Figure 8: (Left) The event mistag rate E_{bc} versus the event correct tag rate E_{cc} for vertex detectors with different inner radius, using the same hit resolution of 5 μm and the same layer thickness of 0.12% X^0. (Right) The corresponding fractional $BR(H \to c\bar{c})$ precision.
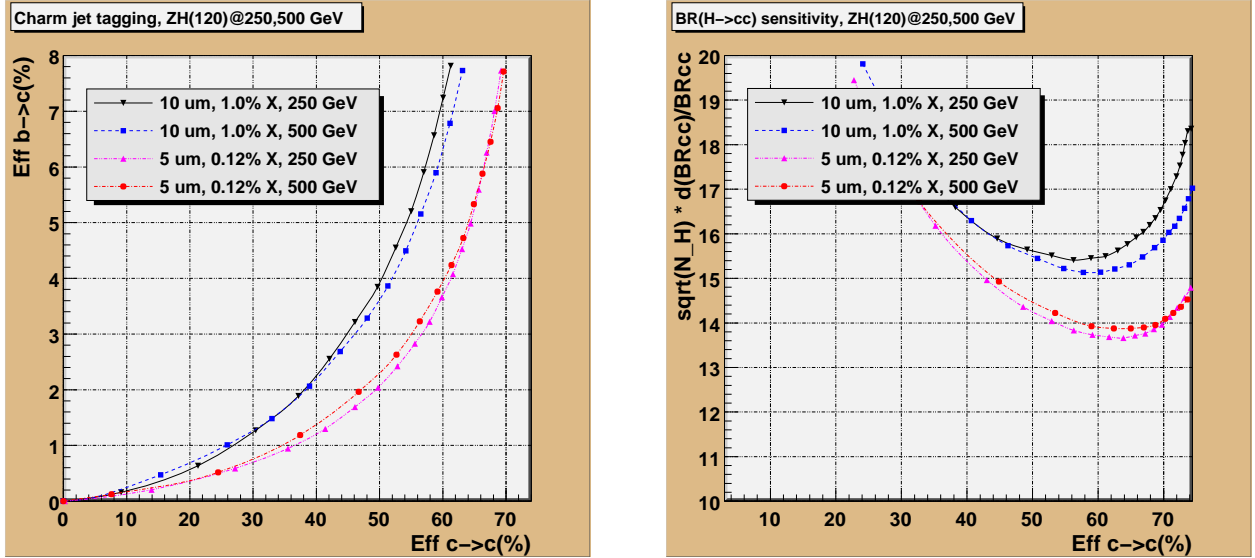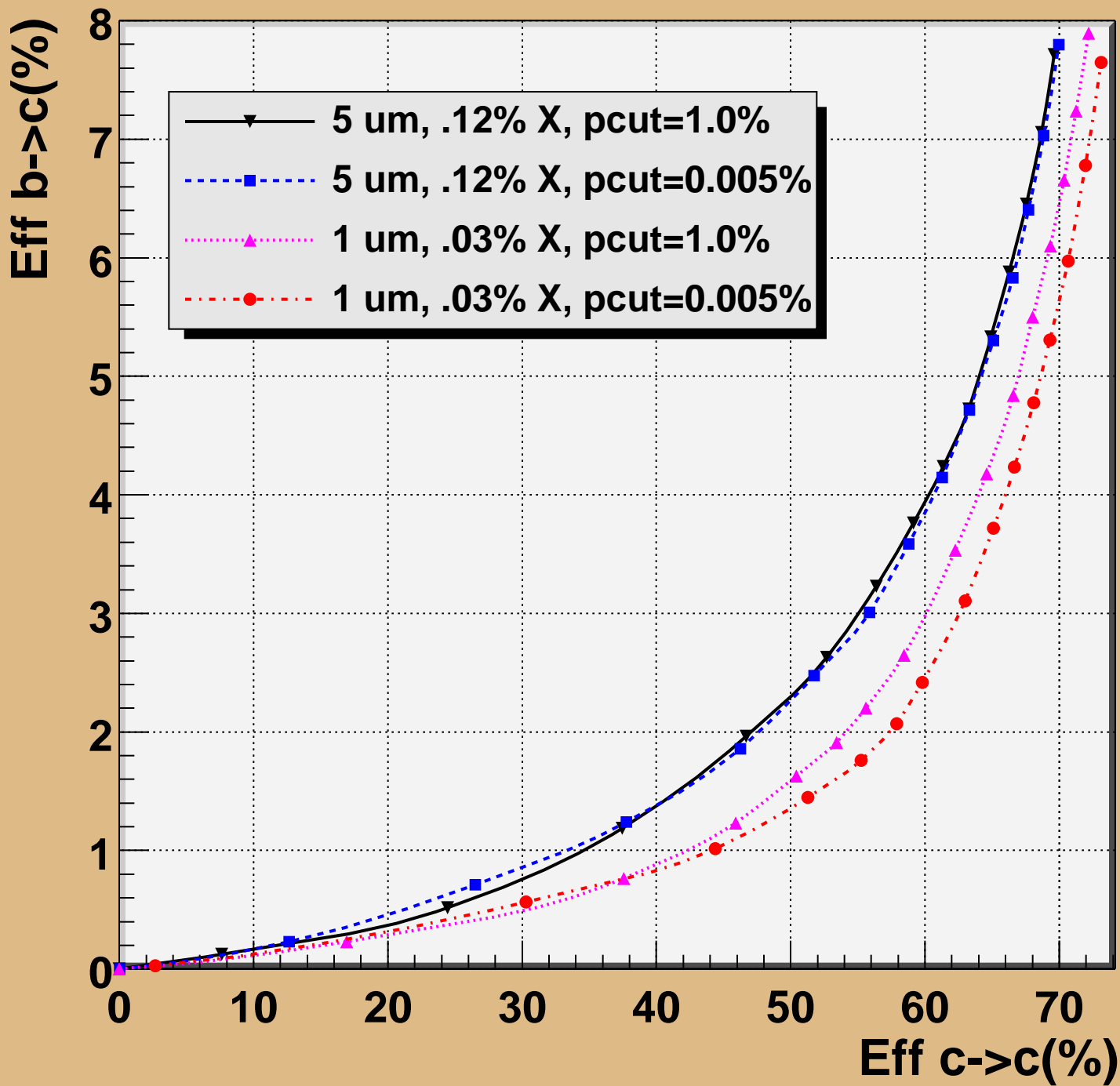

Figure 9: (Left) The event mistag rate E_{bc} versus the event correct tag rate E_{cc} at two different $\sqrt{s}$ for two detector models. The inner radius is kept at 1.2 cm. (Right) The corresponding fractional $BR(H \to c\bar{c})$ precision.

Charm jet tagging, ZH(120)@500 GeV

Legend:
- 5 um, .12% X, pcut=1.0%
- 5 um, .12% X, pcut=0.005%
- 1 um, .03% X, pcut=1.0%
- 1 um, .03% X, pcut=0.005%

X axis: Eff c->c(%)
Y axis: Eff b->c(%)

BR(H->cc) sensitivity, ZH(120)@500 GeV

Legend:
- 5 um, .12% X, pcut=1.0%
- 5 um, .12% X, pcut=0.005%
- 1 um, .03% X, pcut=1.0%
- 1 um, .03% X, pcut=0.005%

Y-axis: sqrt(BRcc*Ecc + BRbb*Ebc + .02)/(Ecc*BRcc)

X-axis: Eff c->c(%)